

## A simple self-assembly strategy for ultrahigh surface area nitrogen-doped porous carbon nanospheres with enhanced adsorption and energy storage performances

Zhiwei Tang, Shaohong Liu, Zhitao Lu, Xidong Lin, Bingna Zheng, Ruliang Liu, Dingcai Wu\* and Ruowen Fu\*

Materials Science Institute, PCFM Lab and GDHPRC Lab, School of Chemistry, Sun Yat-sen University, Guangzhou 510275, P. R. China

E-mail: [wudc@mail.sysu.edu.cn](mailto:wudc@mail.sysu.edu.cn); [cesfrw@mail.sysu.edu.cn](mailto:cesfrw@mail.sysu.edu.cn)

### Experimental section

**Synthesis of PACP/PEO-*b*-PS composite nanospheres and PCNSs.** In a typical synthesis process, 0.17 ml of aniline and 0.13 ml of pyrrole were dissolved in 12 ml of ethanol/deionized water (1:2 by volume) solution. Then the above solution was added into 4 ml of tetrahydrofuran containing 30 mg of PEO<sub>113</sub>-*b*-PS<sub>445</sub> under mild stirring at 0 °C, which instantly form a transparent blue solution. After 1 h, 2 ml of 0 °C precooled aqueous solution containing 0.82 g of ammonium persulphate was added into the above 0 °C precooled transparent blue solution, followed by strong stirring for 50 s. Then the homogeneous mixture solution was polymerized for 12 h at 0 °C on standing. After that, PACP/PEO<sub>113</sub>-*b*-PS<sub>445</sub> composite nanospheres were obtained by filtration and washed with ethanol and deionized water for several times until the filtrate became colorless, followed by drying under vacuum at 50 °C for 24 h. The resulting PACP/PEO<sub>113</sub>-*b*-PS<sub>445</sub> composite nanospheres were treated at 350 °C for 3 h and then at 700-1000 °C for desired carbonization time with different heating rates under N<sub>2</sub> flow in a temperature-programmable tube furnace. The resulting PCNSs were denoted as PCNS-x-yHzR, where x, y and z denotes the carbonization temperature (°C), carbonization time (h) and heating rate (°C min<sup>-1</sup>). On the other hand, PACP/PEO<sub>113</sub>-*b*-PS<sub>142</sub> and PACP/PEO<sub>113</sub>-*b*-PS<sub>250</sub> composite nanospheres were also prepared according the above procedures, except using PEO<sub>113</sub>-*b*-PS<sub>142</sub> and PEO<sub>113</sub>-*b*-PS<sub>250</sub> as templates; and their carbonization at 900 °C for 3 h with 2 °C min<sup>-1</sup> led to formation of PCNSs.

**Preparation of PCNS-900-20H2R/S composite.** PCNS-900-20H2R/S composite was prepared by heating-melting of a mixture of PCNS-900-20H2R and sulfur (4:6 by weight) in a sealed ampoule bottle filled with nitrogen at 155 °C for 20 h in a sealed tube furnace under nitrogen flow (200 ml/min). At 155 °C, the molten sulfur exhibited the lowest viscosity and could easily diffuse into the nanopores of PCNS-900-20H2R, leading to formation of the target PCNS-900-20H2R/S composite.

**Sample characterization.** The nanomorphologies were visualized by using a field emission scanning electron microscopy (FESEM, JSM-6330F) and a transmission electron microscopy (TEM, Tecnai G2 Spirit). Pore structures were determined using a Micromeritics ASAP 2020 instrument at 77 K. Brunauer-Emmett-Teller (BET) and Langmuir surface areas were analyzed according to BET and Langmuir theories, respectively. Pore size distributions were calculated based on the original Density Function Theory (DFT). Thermogravimetric analysis (TGA, NetzschTG-209) was carried out to determine the sulfur content in the PCNS-900-20H2R/S composite. XRD patterns were recorded on a D-MAX 2200 VPC diffractometer using Cu K radiation (40 kV, 26 mA). Raman spectra were measured and collected using a Laser Micro-Raman Spectrometer (Renishaw inVia) with 633 nm laser excitation under ambient conditions. X-ray photoelectron spectroscopy (XPS) measurements were performed on an ESCALab250 instrument.

**Liquid phase adsorption experiment.** Activated carbon was obtained from commercial medicinal charcoal tablets (Aixite, Changtian Pharma) by washing the tablets with deionized water several times to remove the surface coating and drying under vacuum at 60 °C for 24 h. 20 mg of carbon samples (activated carbon or PCNS) were added into a conical flask, and then 40 ml of creatinine solution (100 mg/L) was quickly poured into the conical flask. The resulting suspensions were rapidly transferred to the shaker and shaken under the rate of 150 rpm at 25 °C for scheduled time. The concentration of creatinine was quantitatively measured by UV-Vis absorption spectra at wavelength of 232 nm using diluted supernate (0.3 ml was diluted to 10 ml).

**Electrochemical measurements.** The sulfur cathode slurry was fabricated by mixing 80 wt% PCNS-900-20H2R/S composite, 10 wt% Super P, and 10 wt% polyvinylidene fluoride in *N*-methyl-2-pyrrolidinone (NMP), and then spread onto a piece of carbon coating Al foil substrate (thickness of 18  $\mu\text{m}$ ), followed by drying 12 h under vacuum and cutting into small disks with a diameter of 12 mm. The Li-S cells were assembled with CR2032 coin-type cells with PCNS-900-20H2R/S cathode, commercial polypropylene separator (Celgard 2400), lithium foil anode in an argon-filled glove box with moisture and oxygen content below 1.0 ppm. The used electrolyte was a freshly prepared solution of lithium bis(tri-*uoromethanesulfonyl)imide (1 M) in 1,2-dimethoxyethane and 1,3-dioxolane (1:1 by volume) with 1 wt% LiNO<sub>3</sub> additive. Galvanostatic charging/discharging tests were operated in the potential range of 1.7-2.8 V at room temperature by using LAND CT2001A battery test system.*

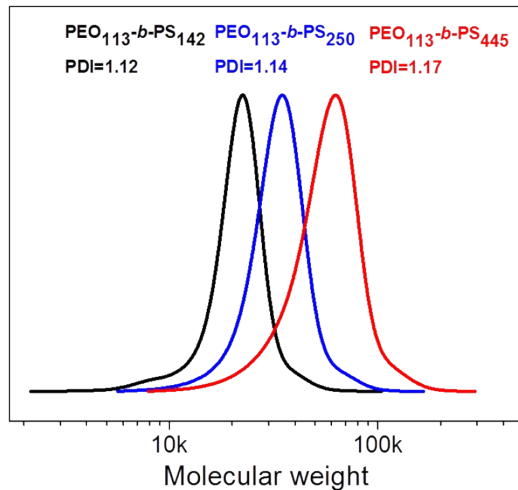


**Fig. S1** GPC traces of  $\text{PEO}_{113}\text{-}b\text{-}\text{PS}_{142}$  (black),  $\text{PEO}_{113}\text{-}b\text{-}\text{PS}_{250}$  (blue) and  $\text{PEO}_{113}\text{-}b\text{-}\text{PS}_{445}$  (red).

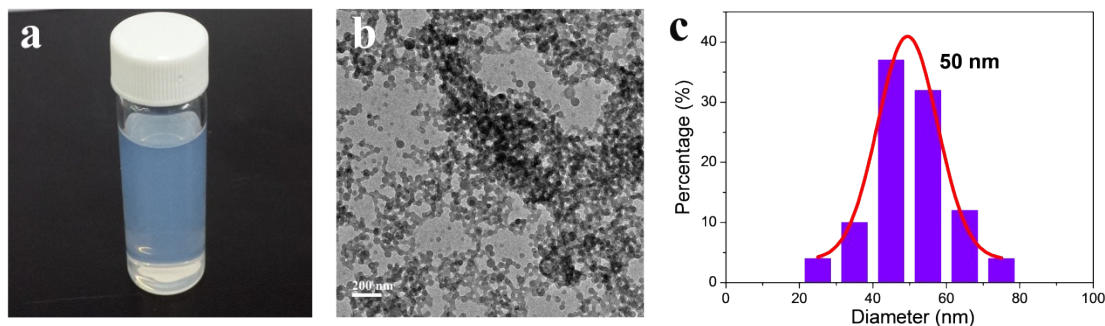


**Fig. S2** (a) Digital photograph, (b) TEM image and (c) diameter distribution histogram of  $\text{PEO}_{113}\text{-}b\text{-}\text{PS}_{445}$  micelles, which were obtained by adding ethanol/deionized water solution of aniline and pyrrole into tetrahydrofuran solution of  $\text{PEO}_{113}\text{-}b\text{-}\text{PS}_{445}$ . Note that the ratio of  $\text{PEO}_{113}\text{-}b\text{-}\text{PS}_{445}$  / tetrahydrofuran / aniline / pyrrole / ethanol / deionized water was 30 mg / 4 ml / 0.17 ml / 0.13 ml / 4 ml / 8 ml.

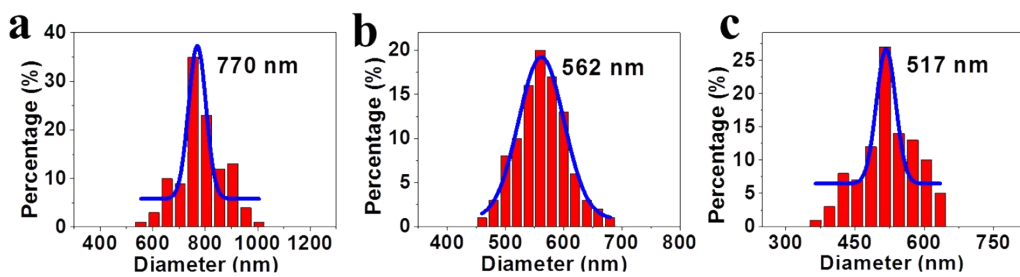


**Fig. S3** Diameter distribution histograms of (a) PACP/ $\text{PEO}_{113}\text{-}b\text{-}\text{PS}_{445}$  composite nanospheres, (b) PCNS-900-3H2R and (c) PCNS-900-20H2R.

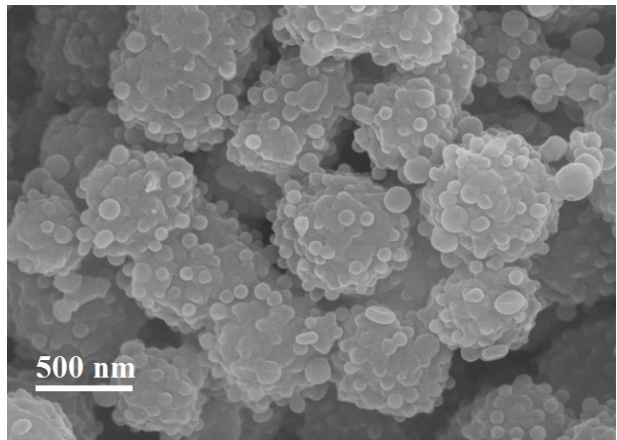


**Fig. S4** High-resolution SEM image of PACP/PEO<sub>113</sub>-*b*-PS<sub>445</sub> composite nanospheres.

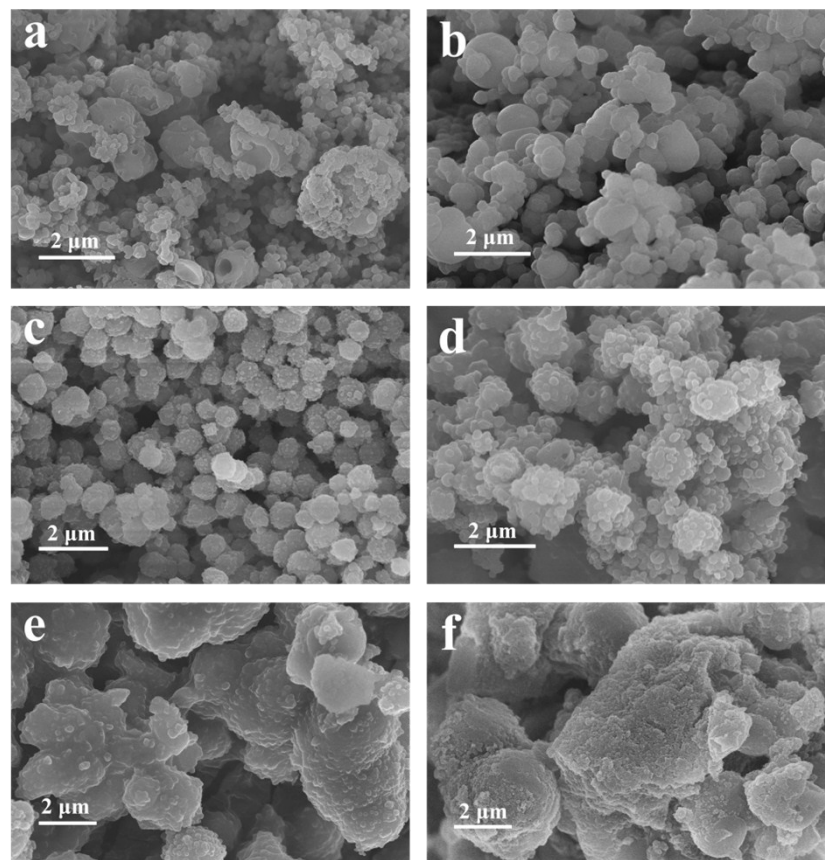


**Fig. S5** SEM images of PACP/PS<sub>445</sub>-*b*-PEO<sub>113</sub> composite products with different solvent ratios of THF / C<sub>2</sub>H<sub>5</sub>OH / H<sub>2</sub>O: (a) 4 ml / 0 ml / 12 ml, (b) 3 ml / 4 ml / 9 ml, (c) 4 ml / 4 ml / 8 ml, (d) 4 ml / 5 ml / 7 ml, (e) 5 ml / 5 ml / 6 ml, and (f) 6 ml / 6 ml / 4 ml. Note that aniline and pyrrole have the same concentration (0.1 M) in all experiments.

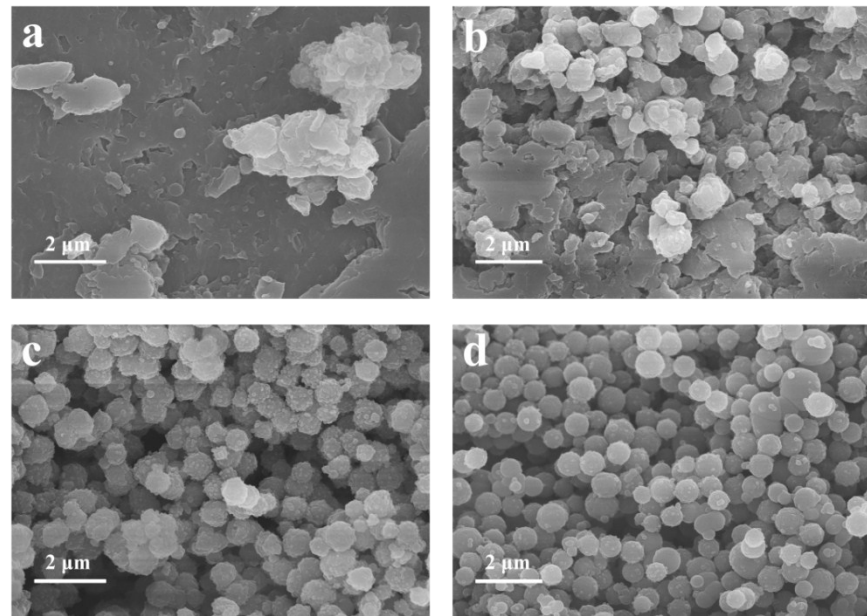


**Fig. S6** SEM images of PACP/PEO<sub>113</sub>-*b*-PS<sub>445</sub> composite products with different concentrations of aniline or pyrrole: (a) 0.04 M, (b) 0.07 M, (c) 0.1 M, and (d) 0.2 M. Note that aniline and pyrrole have the same concentration in all experiments.

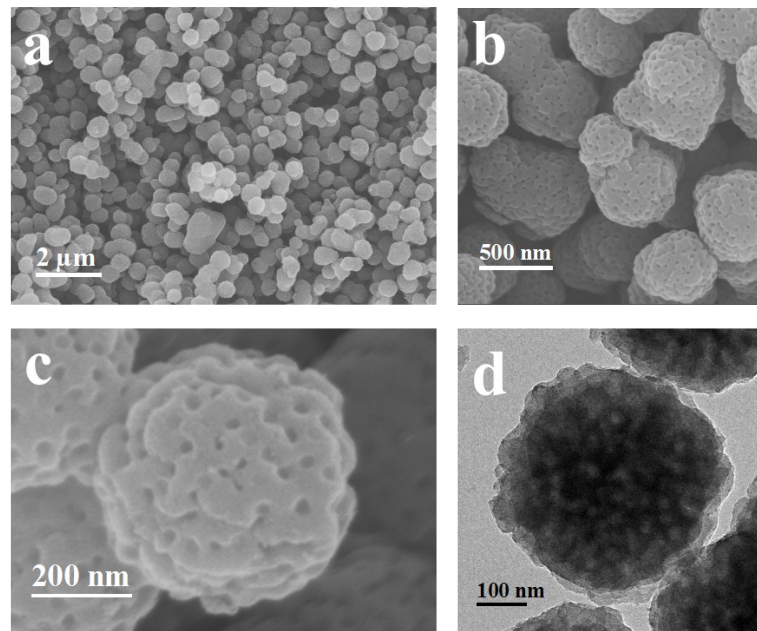


**Fig. S7** (a, b, c) SEM and (d) TEM images of PCNS-900-3H2R.

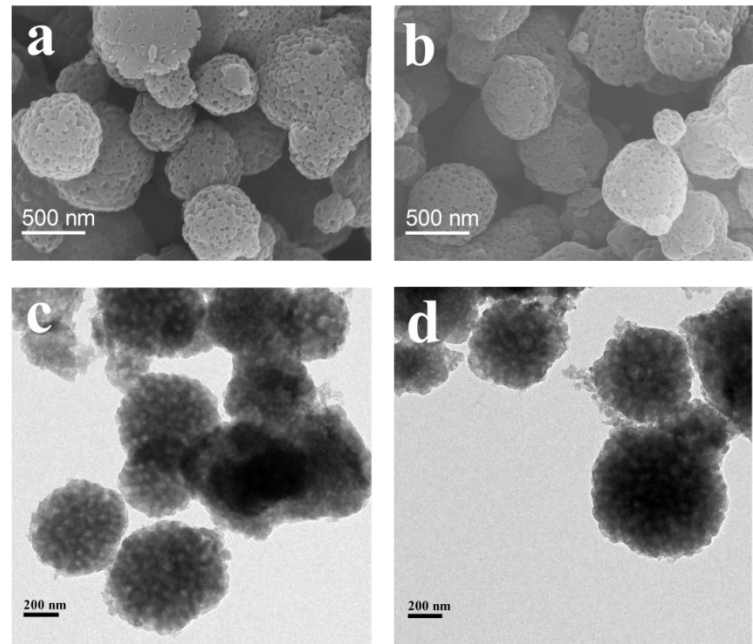


**Fig. S8** SEM images of (a) PCNS-900-6H2R and (b) PCNS-900-10H2R; TEM images of (c) PCNS-900-6H2R and (d) PCNS-900-10H2R.

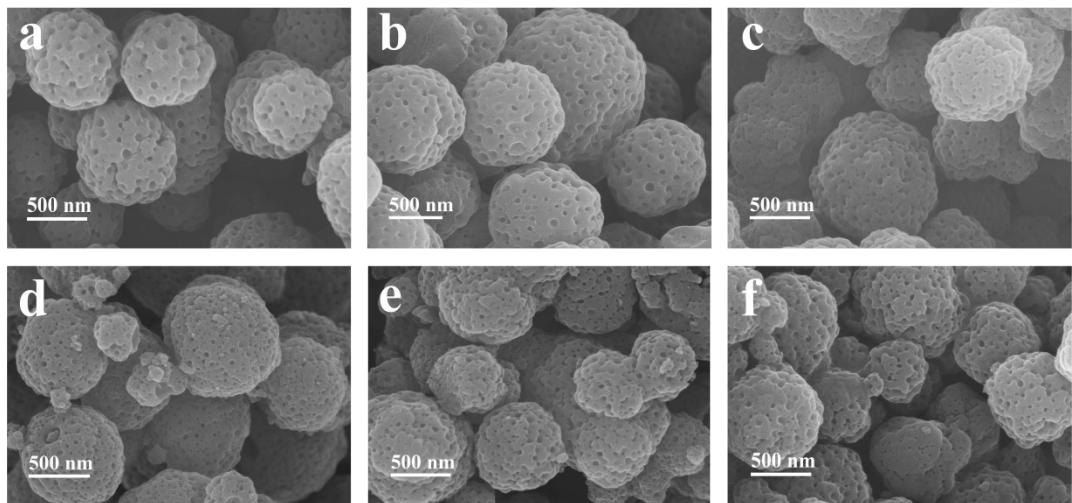


**Fig. S9** SEM images of (a) PCNS-700-3H2R, (b) PCNS-800-3H2R, (c) PCNS-1000-3H2R, (d) PCNS-900-3H1R, (e) PCNS-900-3H5R, and (f) PCNS-900-3H10R.

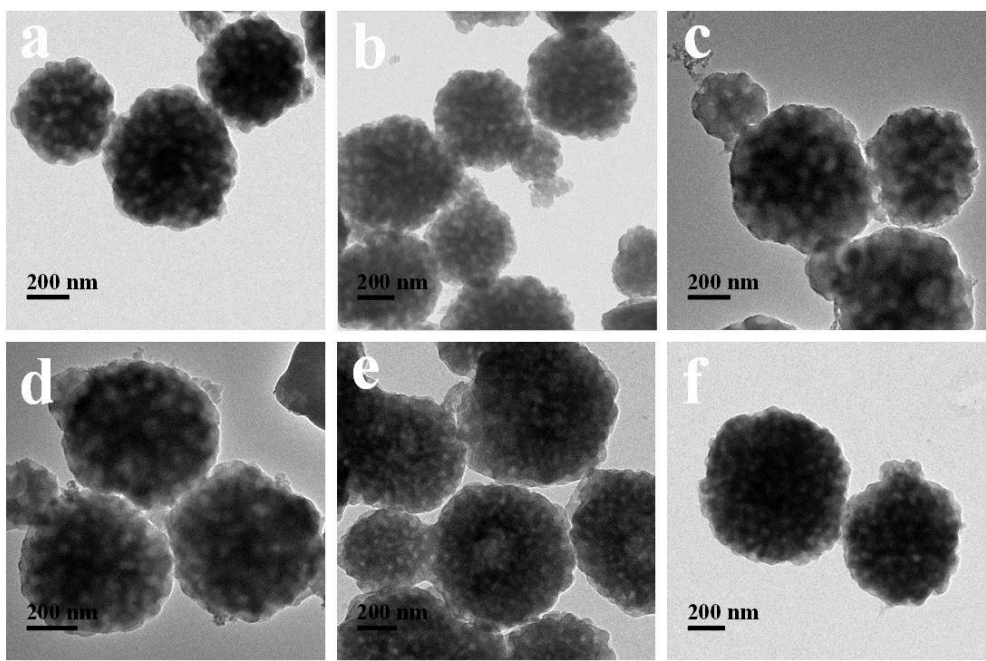


**Fig. S10** TEM images of (a) PCNS-700-3H2R, (b) PCNS-800-3H2R, (c) PCNS-1000-3H2R, (d) PCNS-900-3H1R, (e) PCNS-900-3H5R, and (f) PCNS-900-3H10R.

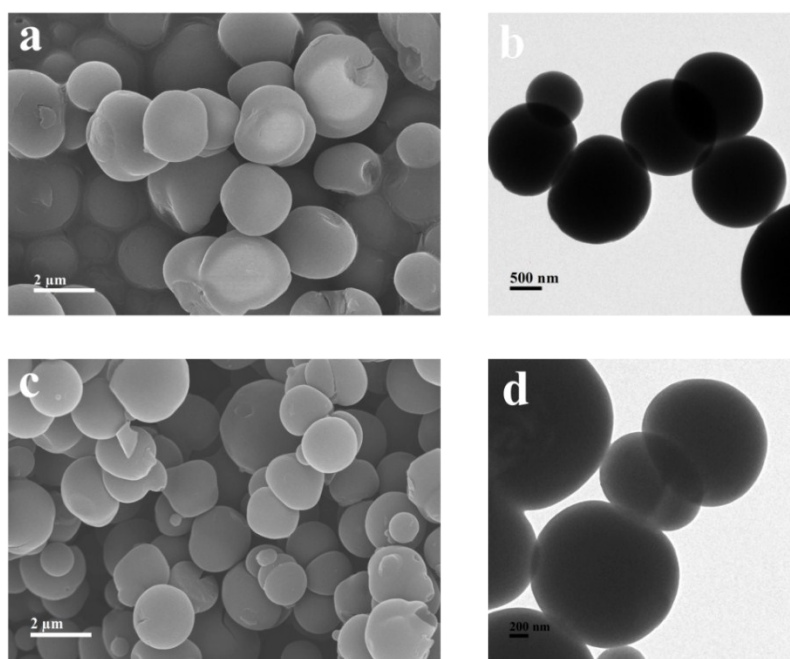


**Fig. S11** SEM (left) and TEM (right) images of (a, b) the PACP control sample without PEO-*b*-PS and (c, d) its corresponding carbon product.

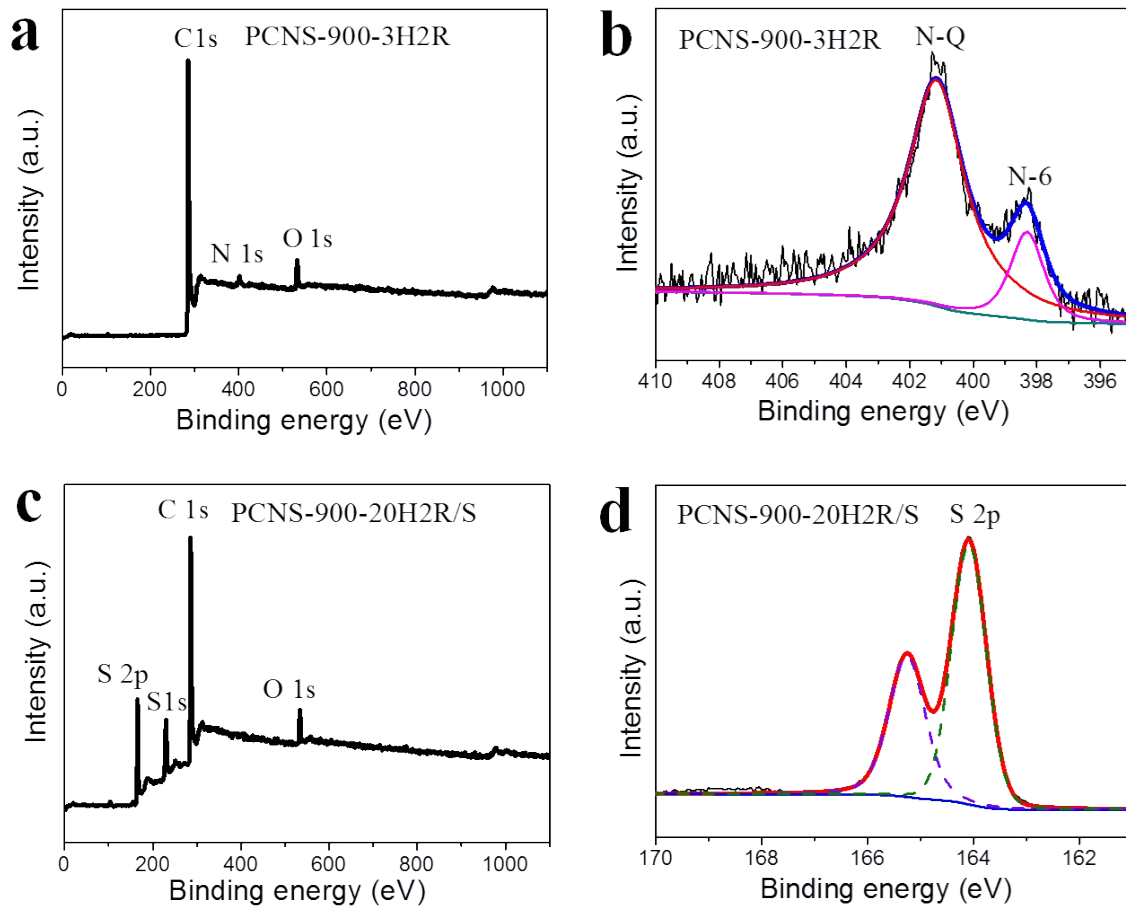


**Fig. S12** The total XPS spectra of (a) PCNS-900-3H2R and (c) PCNS-900-20H2R/S composite; (b) N 1s spectrum of PCNS-900-3H2R; (d) S 2p spectrum of PCNS-900-20H2R/S. The peaks at 164.1 and 165.2 eV in (d) indicate that the uniformly encapsulated sulfur exists in the form of elemental sulfur.

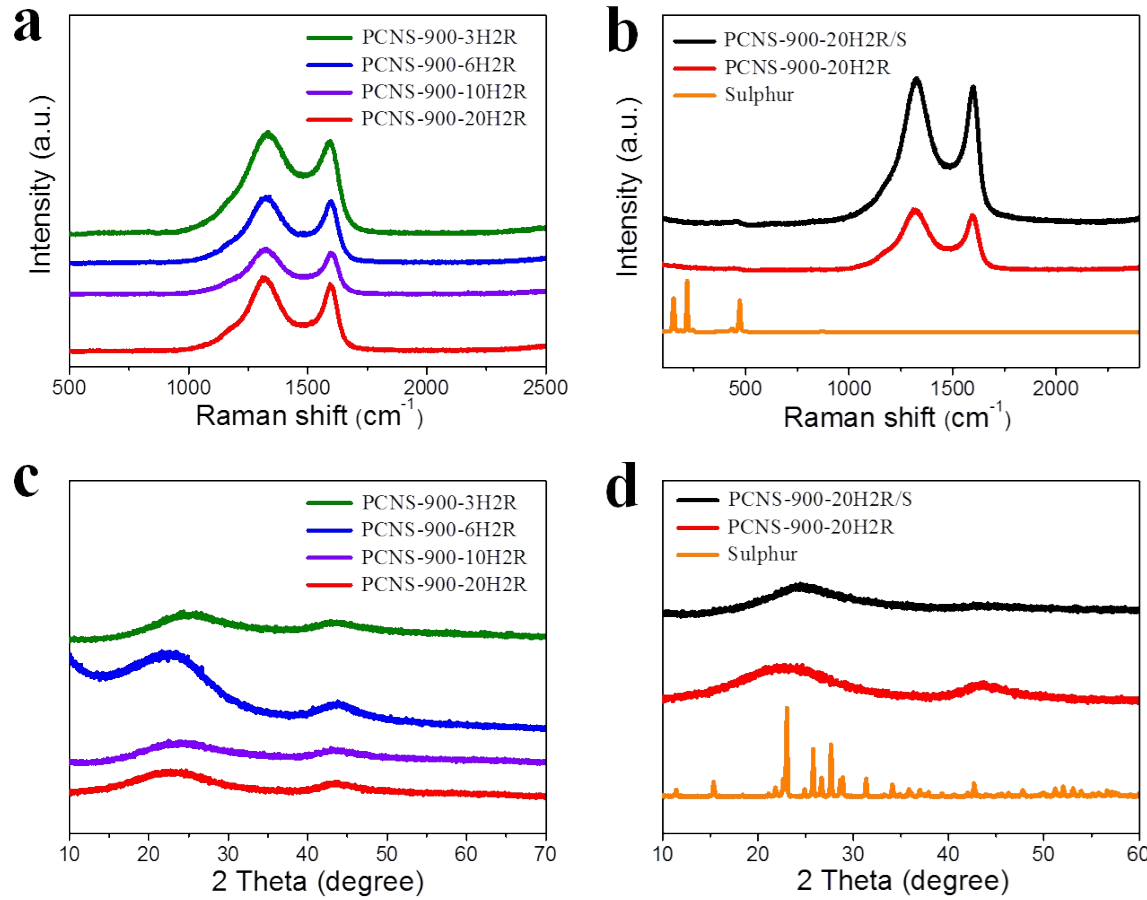


**Fig. S13** Raman spectra of (a) PCNSs with various carbonization times; (b) PCNS-900-20H2R/S, PCNS-900-20H2R and pure sulfur. XRD profiles of (c) PCNSs with various carbonization times; (d) PCNS-900-20H2R/S, PCNS-900-20H2R and pure sulfur. No signals below  $500 \text{ cm}^{-1}$  in (b) are found, and the diffraction signals assignable to crystalline sulfur disappear in (d), confirming that sulfur in PCNS-900-20H2R/S is a homogeneously dispersed state.

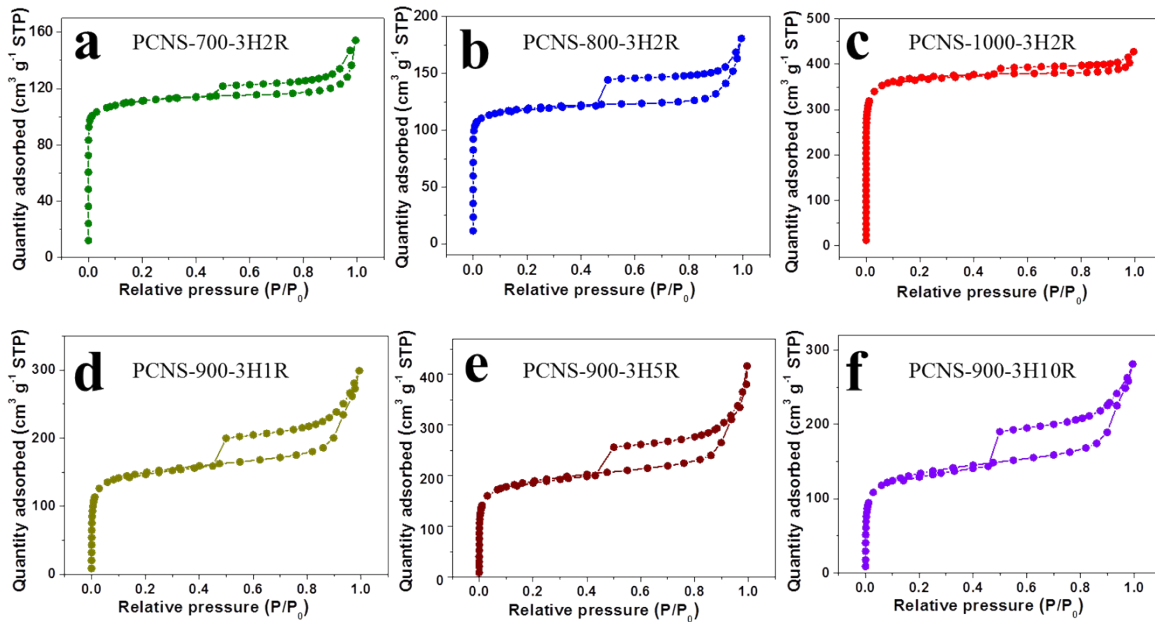


**Fig. S14**  $\text{N}_2$  adsorption-desorption isotherms of PCNSs obtained under various carbonization conditions.

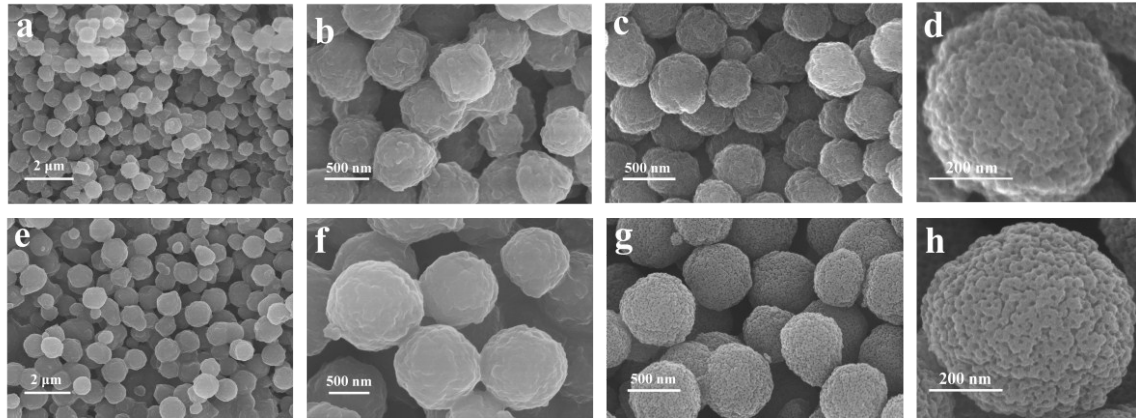


**Fig. S15** SEM images of (a, b) PACP/PS<sub>142</sub>-*b*-PEO<sub>113</sub> composite nanospheres, (c, d) PCNS-PS<sub>142</sub>-*b*-PEO<sub>113</sub>, (e, f) PACP/PS<sub>250</sub>-*b*-PEO<sub>113</sub> composite nanospheres, and (g, h) PCNS-PS<sub>250</sub>-*b*-PEO<sub>113</sub>. Note that PCNS-PS<sub>142</sub>-*b*-PEO<sub>113</sub> and PCNS-PS<sub>250</sub>-*b*-PEO<sub>113</sub> were obtained by carbonization of PACP/PS<sub>142</sub>-*b*-PEO<sub>113</sub> composite nanospheres and PACP/PS<sub>250</sub>-*b*-PEO<sub>113</sub> composite nanospheres at 900 °C for 3 h with 2 °C min<sup>-1</sup>, respectively.

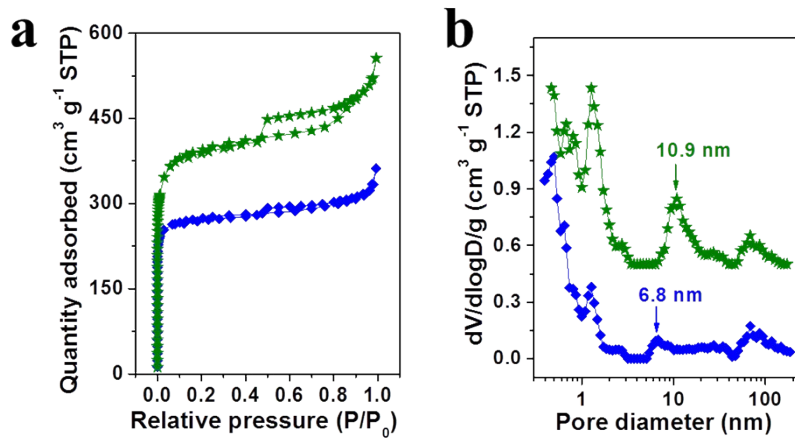


**Fig. S16** (a) N<sub>2</sub> adsorption-desorption isotherms and (b) pore size distribution curves of PCNS-PS<sub>250</sub>-*b*-PEO<sub>113</sub> (green) and PCNS-PS<sub>142</sub>-*b*-PEO<sub>113</sub> (blue).

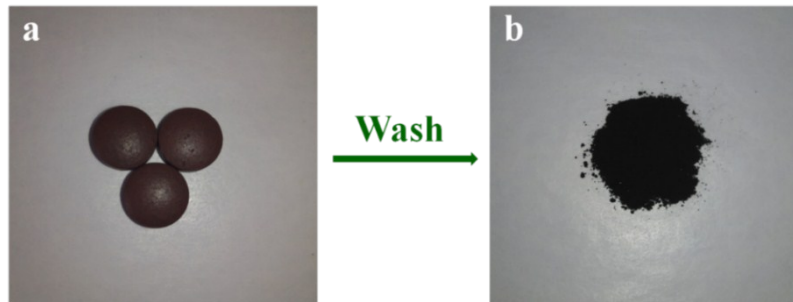


**Fig. S17** Digital photographs of (a) commercial medicinal charcoal tablets, and (b) their active component (i.e., activated carbon powder) obtained by removing the water soluble film coating with deionized water.

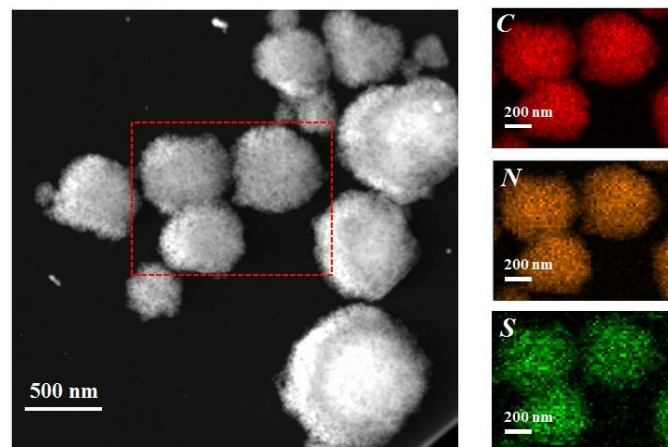


**Fig. S18** High-resolution scanning transmission electron microscopy (STEM) images and the corresponding EDS elemental mappings of carbon (red), nitrogen (orange) and sulfur (green) for PCNS-900-20H2R/S.

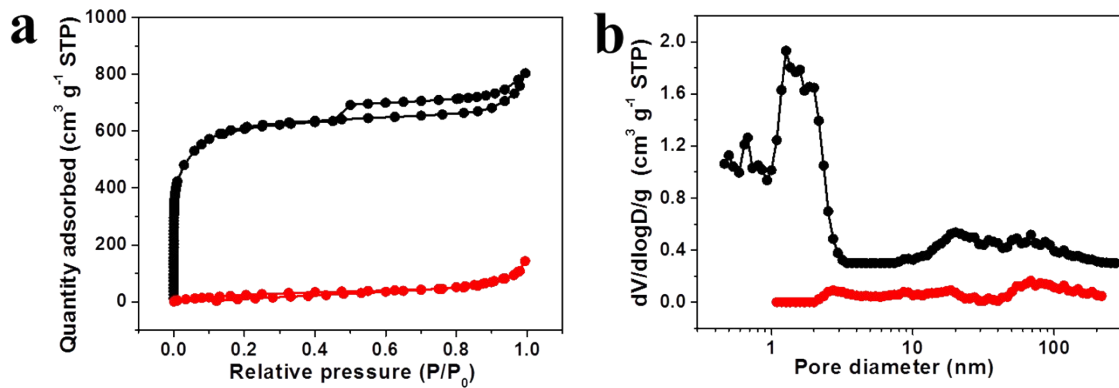


**Fig. S19** (a) Nitrogen adsorption-desorption isotherms and (b) DFT pore size distribution curves for PCNS-900-20H2R (black) and PCNS-900-20H2R/S (red).

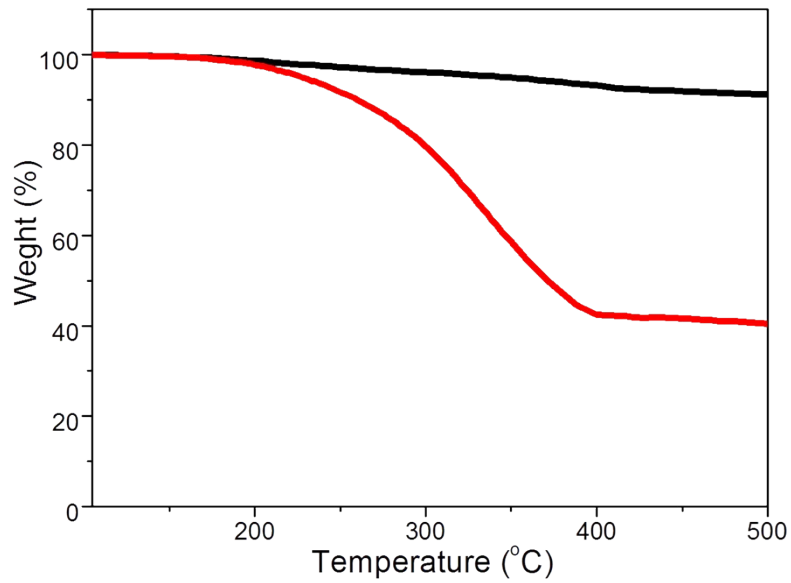


**Fig. S20** TGA curves of PCNS-900-20H2R (black) and PCNS-900-20H2R/S (red), revealing that the sulfur content of PCNS-900-20H2R/S is 50.2%.

**Table S1** Preparation method, sphere diameter,  $S_{BET}$ , mesopore size for mesoporous carbon nanospheres reported previously.

Sample	Preparation method	Sphere diameter (nm)	$S_{BET}$ ( $m^2 g^{-1}$ )	Mesopore size (nm)	Ref.
Mesoporous carbon spheres	Soft-templating	50-1000	760	9	1
MCNs	Soft-templating	20-140	894-1131	3	2
Mesoporous carbon spheres	Hard-templating	180-850	1044-1129	2.4	3
MCNs	Soft-templating	300-350	640-857	3.5	4
N-MCNs	Soft-templating	120	342	/	5
N-oMCNs	Soft-templating	240	446-549	2.8	6
HMCNs	Soft-templating	150	568	9.1	7
NMCS	Soft-templating	164	793	4.2	8
N-MCNs	Soft-templating	165-201	336-759	5.4-16	9
N-MCNs	Hard-templating	98-264	785-1117	7-42	10

**Table S2** Summary of pore parameters for PCNSs.

Sample	$S_{BET}$ ( $m^2 g^{-1}$ )	$S_{Lang}$ ( $m^2 g^{-1}$ )	$S_{mic}$ ( $m^2 g^{-1}$ )	$S_{ext}$ ( $m^2 g^{-1}$ )	$V_{mic}$ ( $cm^3 g^{-1}$ )	$V_t$ ( $cm^3 g^{-1}$ )
PCNS-700-3H2R	372	497	304	68	0.14	0.24
PCNS-800-3H2R	483	640	410	73	0.19	0.32
PCNS-900-3H2R	1019	1352	826	193	0.38	0.68
PCNS-1000-3H2R	1244	1649	1051	193	0.48	0.66
PCNS-900-6H2R	1629	2177	1167	462	0.54	0.98
PCNS-900-10H2R	2277	3072	1398	879	0.63	1.37
PCNS-900-20H2R	2520	3219	1255	1265	0.48	1.43
PCNS-900-3H1R	612	815	548	64	0.25	0.31
PCNS-900-3H5R	723	963	631	92	0.29	0.37
PCNS-900-3H10R	568	756	501	67	0.23	0.29
PCNS-PS <sub>142</sub> - <i>b</i> -PEO <sub>113</sub>	915	1221	757	158	0.35	0.56
PCNS-PS <sub>250</sub> - <i>b</i> -PEO <sub>113</sub>	1337	1779	993	344	0.46	0.86

Note:  $S_{BET}$ ,  $S_{Lang}$ ,  $S_{mic}$ ,  $S_{ext}$ ,  $V_{mic}$  and  $V_t$  denote BET surface area, Langmuir surface area, micropore surface area, external surface area, micropore volume and total pore volume, respectively.

**Table S3** Summary of cycle stability performances for various sulfur host materials.

Sample	Rate	Initial capacity	Cycle number	Retention (%)	Ref.
<b>PCNS-900-20H2R/S</b>	<b>2 C</b>	<b>856</b>	<b>1000</b>	<b>83.5</b>	<b>This work</b>
<b>Mesoporous carbons</b>	S-BMC/S	1 C	1070	100	60.8
	BMC-1/S	1 C	995	100	55.3
	Ordered meso-microporous core-shell carbon/S	0.5 C	1037	200	80
	MC/S	0.1 C	1390	100	60.4
	RGO@CMK-3/S	1 C	956	200	59.6
	OMC /S	2.7 C	761	400	54.5
	Mesoporous carbon spheres/S	0.2 C	1388	100	61.7
	CPAN-800/S	1 C	~1000	100	66.7
	GOMC/S	1 C	869	300	52
<b>Microporous carbons</b>	Microporous carbon spheres/S	0.24 C	800	500	55.1
	(CNT@MPC)/S	0.1 C	1269	200	71.3
	AAC/S	1 C	1193	200	51.4
	Microporous carbon nanosheets/S	0.1 C	1600	50	34.6
	Microporous carbon spheres/S	0.1 C	1200	800	45.8
	Ordered microporous carbon/S	0.24 C	2200	500	34.1
	Microporous bamboo biochar/S	0.48 C	961	150	57.2
<b>Hierarchical porous carbons</b>	HPC/S	1 C	1249	100	45
		2 C	822	100	51
	Hierarchically ordered Porous carbon /S	1 C	650	100	74
	N-HPCC/S	0.48 C	1001	200	60.6
	HPC/S	2.4 C	770	500	77
	TAC-CDC/S	0.5 C	1229	200	58.9

	3D PGC/S	2 C	1115	1000	61	32
<b>Hollow carbon spheres</b>	DHCS/S	0.1 C	1020	100	67.6	33
	N-HCS/S	0.2 C	1141	150	53	34
	GHCS/S	0.5 C	1300	100	79	35
	h-CNS/S	0.5 C	1200	100	52	36
<b>Graphenes</b>	Sandwiched graphene/S	0.9 C	971	300	70	37
	Unstacked double-layer template graphene	1 C	1084	200	64.7	38
	Graphene-wrapped C/S	2 C	606.7	300	80.2	39
	HIPG/S	1 C	914	500	53.2	40
<b>Carbon nanotubes</b>	SDCNT-500/S	0.25 C	~900	100	72.9	41
	VA-CNT/S	0.08 C	~1580	40	50	42
	CNT-S film	0.1 C	1100	100	67.3	43
	VT-CNT/S	1 C	844	450	64	44
	SCNT-300/S	2 C	~820	500	39	45
	HPNACNTs-5/S	2 C	933	200	65	46
<b>Other materials</b>	SPANI-NT/S	1 C	511	500	76	47
	S@PANi yolk-shell	0.5 C	920	200	68.3	48
	TiO <sub>2</sub> /S	0.5 C	1030	1000	67	49
	ZIF-8/S	0.5 C	738	300	75	50
	Ti <sub>2</sub> C/S	0.5 C	1090	400	80	51
	Covalent triazine framework/S	2 C	406.3	300	81	52

## References

1. J. E. Hampsey, Q. Hu, Z. Wu, L. Rice, J. Pang, Y. Lu, *Carbon* 2005, **43**, 2977-2982.
2. Y. Fang, D. Gu, Y. Zou, Z. Wu, F. Li, R. Che, Y. Deng, B. Tu, D. Zhao, *Angew. Chem. Int. Ed.* 2010, **49**, 7987-7991.
3. Z. A. Qiao, B. Guo, A. J. Binder, J. Chen, G. M. Veith, S. Dai, *Nano Lett.* 2013, **13**, 207-212.
4. J. Liu, T. Yang, D. W. Wang, G. Q. Lu, D. Zhao, S. Z. Qiao, *Nat. Commun.* 2013, **4**, 2798.
5. T. Yang, J. Liu, R. Zhou, Z. Chen, H. Xu, S. Z. Qiao, M. J. Monteiro, *J. Mater. Chem.* 2014, **2**, 18139-18146.
6. A. Chen, Y. Yu, Y. Zhang, W. Zang, Y. Yu, Y. Zhang, S. Shen, J. Zhang, *Carbon* 2014, **80**, 19-27.
7. Y. Dai, H. Jiang, Y. Hu, Y. Fu, C. Li, *Ind. Eng. Chem. Res.* 2014, **53**, 3125-3130.
8. J. Wang, H. Liu, J. Diao, X. Gu, H. Wang, J. Rong, B. Zong, D. S. Su, *J. Mater. Chem.* 2015, **3**, 2305-2313.
9. J. Tang, J. Liu, C. Li, Y. Li, M. O. Tade, S. Dai, Y. Yamauchi, *Angew. Chem. Int. Ed.* 2015, **54**, 588-593.
10. G. Wang, Y. Sun, D. Li, H. W. Liang, R. Dong, X. Feng, K. Müllen, *Angew. Chem. Int. Ed.* 2015, **54**, 15191-15196.
11. J. Schuster, G. He, B. Mandlmeier, T. Yim, K. T. Lee, T. Bein, L. F. Nazar, *Angew. Chem. Int. Ed.* 2012, **51**, 3591-3595.
12. G. He, X. Ji, L. Nazar, *Energy Environ. Sci.* 2011, **4**, 2878-2783.
13. Z. Li, Y. Jiang, L. Yuan, Z. Yi, C. Wu, Y. Liu, P. Strasser, Y. Huang, *ACS Nano* 2014, **8**, 9295-9303.
14. X. Li, Y. Cao, W. Qi, L. V. Saraf, J. Xiao, Z. Nie, J. Mietek, J. G. Zhang, B. Schwenzer, J. Liu, *J. Mater. Chem.* 2011, **21**, 16603-16610.
15. S. Chen, Q. Tang, X. Chen, A. Hu, W. Deng, Z. Liu, *RSC Adv.* 2015, **5**, 74138-74143.
16. S. R. Chen, Y. P. Zhai, G. L. Xu, Y. X. Jiang, D. Y. Zhao, J. T. Li, L. Huang, S. G. Sun, *Electrochim. Acta* 2011, **56**, 9549-9555.
17. D. Wang, A. Fu, H. Li, Y. Wang, P. Guo, J. Liu, X. S. Zhao, *J. Power Sources* 2015, **285**, 469-477.
18. Y. Liu, X. Zhao, G. S. Chauhan, J. H. Ahn, *Appl. Surf. Sci.* 2016, **380**, 151-158.
19. M. S. Kim, J. Jeong, W. Cho, W. Kim, *Nanotechnology* 2016, **27**, 125401.
20. B. Zhang, X. Qin, G. R. Li, X. P. Gao, *Energy Environ. Sci.* 2010, **3**, 1531-1537.
21. S. Xin, L. Gu, N. H. Zhao, Y. X. Yin, L. J. Zhou, Y. G. Guo, L. J. Wan, *J. Am. Chem. Soc.* 2012, **134**, 18510-18513.
22. K. Yang, Q. Gao, Y. Tan, W. Tian, L. Zhu, C. Yang, *Micropor. Mesopor. Mat* 2015, **204**, 235-

241.

23. J. Guo, J. Zhang, F. Jiang, S. Zhao, Q. Su, G. Du, *Electrochim. Acta* 2015, **176**, 853-860.
24. S. Zheng, Y. Chen, Y. Xu, F. Yi, Y. Zhu, Y. Liu, J. Yang, C. Wang, *ACS Nano* 2013, **7**, 10995-11003.
25. Z. Li, L. Yuan, Z. Yi, Y. Sun, Y. Liu, Y. Jiang, Y. Shen, Y. Xin, Z. Zhang, Y. Huang, *Adv. Energy Mater.* 2014, **4**, 1-8.
26. X. Gu, Y. Wang, C. Lai, J. Qiu, S. Li, Y. Hou, W. Martens, N. Mahmood, S. Zhang, *Nano Research* 2015, **8**, 129-139.
27. G. Xu, B. Ding, P. Nie, L. Shen, H. Dou, X. Zhang, *ACS Appl. Mater. Interfaces* 2014, **6**, 194-199.
28. B. Ding, C. Yuan, L. Shen, G. Xu, P. Nie, X. Zhang, *Chemistry-A European Journal* 2013, **19**, 1013-1019.
29. J. Yang, S. Wang, Z. Ma, Z. Du, C. Li, J. Song, G. Wang, G. Shao, *Electrochim. Acta* 2015, **159**, 8-15.
30. D. S. Jung, T. H. Hwang, J. H. Lee, H. Y. Koo, R. A. Shakoor, R. Kahraman, Y. N. Jo, M. S. Park, J. W. Choi, *Nano Lett.* 2014, **14**, 4418-4425.
31. Y. Wei, Y. Tao, C. Zhang, J. Wang, W. Qiao, L. Ling, D. Long, *Electrochim. Acta* 2016, **188**, 385-392.
32. G. Li, J. Sun, W. Hou, S. Jiang, Y. Huang, J. Geng, *Nat. Commun.* 2016, **7**, 10601.
33. C. Zhang, H. B. Wu, C. Yuan, Z. Guo, X. W. Lou, *Angew. Chem. Int. Ed.* 2012, **51**, 9592-9595.
34. W. Zhou, X. Xiao, M. Cai, L. Yang, *Nano Lett.* 2014, **14**, 5250-5256.
35. E. S. Shin, M. S. Kim, W. I. Cho, S. H. Oh, *Nanoscale Research Letters* 2013, **8**, 1-8.
36. H. H. Nersisyan, S. H. Joo, B. U. Yoo, D. Y. Kim, T. H. Lee, J. Y. Eom, C. Kim, K. H. Lee, J. H. Lee, *Carbon* 2016, **103**, 255-262.
37. G. Zhou, S. Pei, L. Li, D. W. Wang, S. Wang, K. Huang, L. C. Yin, F. Li, H. M. Cheng, *Adv. Mater.* 2014, **26**, 625-631.
38. M. Q. Zhao, Q. Zhang, J. Q. Huang, G. L. Tian, J. Q. Nie, H. J. Peng, F. Wei, *Nat. Commun.* 2014, **5**, 4410.
39. M. Yu, R. Li, Y. Tong, Y. Li, C. Li, J. D. Hong, G. Shi, *J. Mater. Chem.* 2015, **3**, 9609-9615.
40. W. Qian, Q. Gao, K. Yang, W. Tian, Y. Tan, C. Yang, H. Zhang, Z. Li, L. Zhu, *Energy Technology* 2016, **4**, 625-632.
41. J. Guo, Y. Xu, C. Wang, *Nano Lett.* 2011, **11**, 4288-4294.
42. S. Dorfler, M. Hagen, H. Althues, J. Tubke, S. Kaskel, M. J. Hoffmann, *Chem. Commun.* 2012, **48**, 4097- 4099.
43. K. Jin, X. Zhou, L. Zhang, X. Xin, G. Wang, Z. Liu, *J. Phys. Chem. C* 2013, **117**, 21112-21119.
44. M. Q. Zhao, H. J. Peng, G. L. Tian, Q. Zhang, J. Q. Huang, X. B. Cheng, C. Tang, F. Wei, *Adv.*

*Mater.* 2014, **26**, 7051-7058.

45. J. Yan, X. Liu, X. Wang, B. Li, *J. Mater. Chem.* 2015, **3**, 10127-10133.
46. W. Deng, A. Hu, X. Chen, S. Zhang, Q. Tang, Z. Liu, B. Fan, K. Xiao, *J. Power Sources* 2016, **322**, 138-146.
47. L. Xiao, Y. Cao, J. Xiao, B. Schwenzer, M. H. Engelhard, L. V. Saraf, Z. Nie, G. J. Exarhos, J. Liu, *Adv. Mater.* 2012, **24**, 1176-1181.
48. W. Zhou, Y. Yu, H. Chen, F. J. DiSalvo, H. D. Abruña, *J. Am. Chem. Soc.* 2013, **135**, 16736-16743.
49. Z. Wei Seh, W. Li, J. J. Cha, G. Zheng, Y. Yang, M. T. McDowell, P. C. Hsu, Y. Cui, *Nat. Commun.* 2013, **4**, 1331.
50. J. Zhou, R. Li, X. Fan, Y. Chen, R. Han, W. Li, J. Zheng, B. Wang, X. Li, *Energy Environ. Sci.* 2014, **7**, 2715-2724.
51. X. Liang, A. Garsuch, L. F. Nazar, *Angew. Chem. Int. Ed.* 2015, **54**, 3907-3911.
52. S. N. Talapaneni, T. H. Hwang, S. H. Je, O. Buyukcakir, J. W. Choi, A. Coskun, *Angew. Chem. Int. Ed.* 2016, **128**, 3158-3163.